Monthly Notices
of the
ROYAL ASTRONOMICAL SOCIETY

Mon. Not. R. Astron. Soc. **404,** 134–143 (2010) doi:10.1111/j.1365-2966.2010.16297.x

Magnetic field regulated infall on the disc around the massive protostar Cepheus A HW2

W. H. T. Vlemmings,[1⋆] G. Surcis,[1,2] K. J. E. Torstensson[3,4] and H. J. van Langevelde[3,4]

[1]*Argelander-Institut für Astronomie, University of Bonn, Auf dem Hügel 71, D-53121 Bonn, Germany*
[2]*Max-Planck-Institut für Radioastronomie, Auf dem Hügel 69, D-53121 Bonn, Germany*
[3]*Leiden Observatory, Leiden University, PO Box 9513, NL-2300 RA Leiden, the Netherlands*
[4]*Joint Institute for VLBI in Europe, PO Box 2, NL-7990 AA Dwingeloo, the Netherlands*

Accepted 2010 January 5. Received 2009 December 28; in original form 2009 September 7

ABSTRACT

We present polarization observations of the 6.7-GHz methanol masers around the massive protostar Cepheus A HW2 and its associated disc. The data were taken with the Multi-Element Radio Linked Interferometer Network. The maser polarization is used to determine the full three-dimensional magnetic field structure around Cepheus A HW2. The observations suggest that the masers probe the large-scale magnetic field and not isolated pockets of a compressed field. We find that the magnetic field is predominantly aligned along the protostellar outflow and perpendicular to the molecular and dust disc. From the three-dimensional magnetic field orientation and measurements of the magnetic field strength along the line of sight, we are able to determine that the high-density material, in which the masers occur, is threaded by a large-scale magnetic field of ∼23 mG. This indicates that the protostellar environment at ∼1000 au from Cepheus A HW2 is slightly supercritical ($\lambda \approx 1.7$) and the relation between density and magnetic field is consistent with the collapse along the magnetic field lines. Thus, the observations indicate that the magnetic field likely regulates accretion on to the disc. The magnetic field dominates the turbulent energies by approximately a factor of 3 and is sufficiently strong to be the crucial component stabilizing the massive accretion disc and sustaining the high accretion rates needed during massive star formation.

Key words: magnetic fields – masers – polarization – stars: formation – ISM: individual: Cepheus A.

1 INTRODUCTION

Massive stars are short lived, yet they dominate galaxy evolution due to their strong radiation while enriching the interstellar medium with heavy elements when they explode in a supernova. Massive stars typically form in distant, dense clusters. In such regions, gravitational, radiation and turbulent energies are different from those in the regions that form lower mass stars such as the Sun. Specifically, young stars more massive than $8\,M_{\odot}$ have a radiation pressure that would be sufficient to halt infall and prevent the accretion of additional mass (e.g. Wolfire & Cassinelli 1987). Still, stars more massive than $200\,M_{\odot}$ have been observed (e.g. Figer et al. 1998), indicating that the processes governing massive star formation are yet poorly understood.

A number of different formation scenarios have been proposed (Zinnecker & Yorke 2007). These include formation through the merger of less massive stars (Bonnell & Bate 2005) or through the accretion of unbound gas from the molecular cloud, the competitive accretion theory (Bonnell, Bate & Zinnecker 1998). In the third scenario, core accretion (McKee & Tan 2003), massive stars form through gravitational collapse, which involves disc-assisted accretion to overcome radiation pressure. This scenario is similar to the favoured picture of low-mass star formation (Shu et al. 1995), in which magnetic fields are thought to play an important role by removing excess angular momentum, thereby allowing accretion to continue on to the star (Basu & Mouschovias 1994; Shu et al. 1995). However, the accretion rates during massive star formation are significantly higher than during the formation of a low-mass star, and it is unclear whether massive accretion discs are able to sustain these rates without support by strong magnetic fields (McKee & Tan 2003). Still, if such magnetized discs exist around massive protostars, outflows will arise as a natural consequence (Banerjee & Pudritz 2007).

⋆E-mail: wouter@astro.uni-bonn.de

Current observations of magnetic fields in massive star formation regions are often limited to low-density regions (hydrogen number density $n_{H_2} < 10^6$ cm^{-3}) and/or envelopes at scales of several 1000 au. Linear polarization observations of dust also only provide information on the magnetic field in the plane of the sky, so they have been yet unable to probe the strength and the full structure of the magnetic field close to the protostar and around protostellar discs. Recent high angular resolution submillimetre dust polarization observations of the massive hot molecular core G31.41+0.31 indicate that the gravitational collapse shows signs of being controlled by the magnetic field scales of ∼5000 au (Girart et al. 2009). Currently, the only probes of magnetic fields in the high-density regions close to the massive protostars are masers. Because of their compactness and high brightness, masers are specifically suited for high angular resolution observations of weak linear and circular polarization and can thus be used to determine the magnetic field strength and morphology down to au scales (see Vlemmings 2007, for a review of maser polarization). Most observations have focused on OH and H_2O masers (e.g. Bartkiewicz et al. 2005; Vlemmings et al. 2006a), but recently, methanol masers have been shown to be excellent probes of the magnetic field (e.g. Vlemmings, Harvey-Smith & Cohen 2006b; Vlemmings 2008; Surcis et al. 2009). A number of both OH and methanol maser observations indicate that, although individual maser features are only a few au in size, they probe the large-scale magnetic field around the massive protostar (e.g. Surcis et al. 2009).

We observed Cepheus A, which, at a distance of 700 pc (Moscadelli et al. 2009), is one of the closest regions of active massive star formation. Located in the Cepheus OB3 complex, it hosts a powerful extended bipolar molecular outflow that likely originates from HW2, the brightest radio continuum source in the region (Hughes & Wouterloot 1984). HW2 is thought to be a young protostar of spectral type B0.5 with a mass of ∼20 $M_\odot$ (Jiménez-Serra et al. 2007). The extended outflow appears to be driven by a small-scale (∼700 au) thermal radio jet, with ionized gas ejected at a velocity of ∼500 km s^{-1} (Curiel et al. 2006). In addition to the bipolar outflow, Cepheus A HW2 is surrounded by a rotating disc of dust and molecular gas oriented perpendicular to the jet (Patel et al. 2005; Jiménez-Serra et al. 2007; Torrelles et al. 2007). The jet and disc structure support the picture where massive stars form through disc accretion, similar to low-mass stars. The environment of Cepheus A HW2, however, is significantly more complex than that of typical low-mass protostars. Besides HW2, at least three additional young stellar objects are located within an area of ∼500 × 500 au^2. All these sources seem to be located within or close to the molecular disc (Comito et al. 2007; Torrelles et al. 2007; Jiménez-Serra et al. 2009). The presence of OH, H_2O and CH_3OH (methanol) masers in or near to the disc of Cepheus A HW2 gives us an unique opportunity to study its magnetic field (Bartkiewicz et al. 2005; Vlemmings et al. 2006a), with recent methanol maser Zeeman splitting measurements revealing a dynamically important magnetic field with a ∼8 mG component along the maser line of sight (Vlemmings 2008).

In Section 2, we present the methanol maser observations and in Section 3, we shortly discuss the radiative transfer tool used to infer the full three-dimensional magnetic field geometry. Section 4 presents the results of our observations and in Section 5, we discuss the derived three-dimensional magnetic field morphology and what its implication for the role of the magnetic field during high-mass star formation. Additionally, we highlight the potential for methanol maser polarization observations of the upgraded Multi-Element Radio Linked Interferometer Network (e-MERLIN).

2 OBSERVATIONS

The 5_1–6_0 A^+ maser transition of methanol at 6.7 GHz was observed on 2006 December 2–4 using six of the MERLIN telescopes. Total on source time was ∼27 h, which was interleaved with observations of the phase-calibrator source 2300+638. The resulting beam size was 40 × 30 mas^2. We used a 250 kHz bandwidth with 256 channels for a total velocity coverage of ∼11 km s^{-1} centred on the source velocity $V_{LSR} = -3$ km s^{-1}. This provided a velocity resolution of 0.044 km s^{-1}. To obtain the linear polarization, the data were correlated with the full Stokes parameters. For calibration purposes, the continuum calibrators were observed with the 16 MHz wide-band mode. Both 3C 84 and 3C 286 were also observed in the narrow-band spectral line configuration and were used to determine the phase offset between the wide- and narrow-band set-up. Flux and bandpass calibration was done using the primary flux calibrator 3C 286. Instrumental feed polarization was determined using the unpolarized calibrator 3C 84, and the polarization angle was calibrated using 3C 286. The residual instrumental linear polarization was determined to be <0.1 per cent from the observations of 3C 84 and 2300+638. Self-calibration, in right-circular polarization and left-circular polarization separately, was performed on the strongest isolated maser feature. After calibration, the antenna contributions were reweighted according to their sensitivity at 5 GHz and their individual efficiency. Finally, 5.12 × 5.12 arcsec^2 image cubes were created in Stokes I, Q and U. The rms noise in the emission free channels was ∼6 mJy beam^{-1} for Stokes I and ∼9 mJy beam^{-1} for Stokes Q and U. For the channels with strong maser emission, we are limited to a dynamic range of ∼850 due to residual calibration errors. Because of the dynamic range limit, we were unable to determine the circular polarization due to Zeeman splitting in these observations. The non-detection of the ∼0.17 per cent circular polarization observed for the 6.7-GHz methanol masers using the Effelsberg 100-m telescope (Vlemmings 2008) is unsurprising considering the rms noise limits of our circular polarization observations ($1\sigma \sim 0.12$ per cent).

3 MASER POLARIZATION RADIATIVE TRANSFER

Maser theory describes that the fractional linear polarization P_l of the non-paramagnetic maser species such as H_2O, SiO and CH_3OH, depends on the degree of maser saturation and the angle θ between the maser propagation direction and the magnetic field. Additionally, the relation between the measured polarization angle χ and the magnetic field angle on the sky ϕ_B also depends on θ, with the polarization vectors generally parallel to the field for $\theta < \theta_{crit} \approx 55^\circ$ and perpendicular to the field for $\theta > \theta_{crit}$ (Goldreich, Keeley & Kwan 1973). However, non-magnetic effects, such as full maser saturation and anisotropic maser pumping, can generate enhanced linear polarization and can rotate the polarization vectors with respect to the magnetic field (Deguchi & Watson 1990). Thus, before we can use polarization observations to determine the magnetic field morphology, we need to estimate the level at which these effects influence our measurements. The rotation and generation of linear polarization depends on the amount of Zeeman splitting and the level of maser saturation described by the Zeeman frequency shift $g\Omega$, the maser decay rate Γ and the stimulated emission rate R. When $g\Omega \gg \Gamma > R$, the linear polarization direction is determined by the magnetic field, even in the presence of anisotropic pumping. When the effect of anisotropic pumping is not significant, even $g\Omega > \Gamma$ is a sufficient condition (Watson 2002). The maser

stimulated emission rate is given by

$$R \simeq AkT_{\rm b}\Delta\Omega/4\pi h\nu. \quad (1)$$

Here, A is the Einstein coefficient for the maser transition, which is equal to $0.1532 \times 10^{-8}\,{\rm s}^{-1}$, and k and h are the Boltzmann and Planck constants, respectively. The maser frequency is denoted by ν, and $T_{\rm b}$ and $\Delta\Omega$ are the maser brightness temperature and beaming solid angle, respectively. We measure $T_{\rm b} < 10^{10}$ K for our masers, assuming that they are almost resolved with the MERLIN beam of $\sim$30 mas. However, when observed at even higher angular resolution, more typical sizes are of the order of a few mas and brightness temperatures reach 10^{12} K (Menten et al. 1992). The beaming angle $\Delta\Omega$ cannot easily be measured directly. Still, those of H_2O masers in star-forming regions are shown to be $\Delta\Omega \sim 10^{-4}$–$10^{-5}$ (Nedoluha & Watson 1991), while those in the envelopes of evolved stars are of order 10^{-2} (Vlemmings & van Langevelde 2005). It is likely that methanol masers have similar beaming angles. Taking $\Delta\Omega \sim 10^{-2}$ as a conservative upper limit, the maser stimulated emission rate $R < 0.04\,{\rm s}^{-1}$.

The maser decay rate Γ is more difficult to determine. Maser transitions involved infrared pumping, which includes methanol, $\Gamma \sim 1\,{\rm s}^{-1}$ (Scappaticci & Watson 1992). However, infrared trapping can reduce this value, although likely not by more than an order of magnitude (Goldreich & Kwan 1974). Alternatively, when the maser transition involves collisions, $\Gamma = 0.1 n_{\rm H_2}/10^9\,{\rm s}^{-1}$, with $n_{\rm H_2}$, the hydrogen number density in ${\rm cm}^{-3}$. For the methanol masers, this would imply $\Gamma < 0.1\,{\rm s}^{-1}$. However, as the collisional decay rate is smaller than the radiative decay rate, the radiative decay rate determined Γ. We thus assume $\Gamma = 1\,{\rm s}^{-1}$, though other authors have assumed the lower value of $\Gamma = 0.6\,{\rm s}^{-1}$ (Minier, Booth & Conway 2002).

We have thus shown that even with conservative estimates for R and Γ, we are in the regime where $\Gamma > R$. However, we need to assess if $g\Omega$ is sufficiently much larger than R and Γ so that, even in the case of anisotropic pumping, the polarization vectors can be used to determine the magnetic field direction. The analysis by Nedoluha & Watson (1990) indicates that the effect of anisotropic pumping decreases significantly for transitions with high angular momentum, such as the 6.7-GHz methanol masers. This is further confirmed by the fact that we do not observe any relation between the maser total intensity and fractional polarization, which would be expected when non-magnetic effects contribute to the polarization. However, even without having consider anisotropic pumping, the quantization axis of the maser is potentially not sufficiently determined by the magnetic field when $g\Omega$ is not significantly larger than R and Γ. For a magnetic field strength of $>$8 mG in the Cepheus A methanol maser region (Vlemmings 2008), $g\Omega > 10\,{\rm s}^{-1}$. Although the uncertainty on the magnetic field determination was estimated to be of order 25 per cent, the limit of 8 mG assumes a magnetic field along the maser line of sight and the true magnetic field, and consequently $g\Omega$, will thus likely be larger. Nedoluha & Watson (1990) found that, for a ratio $R/\Gamma < 0.1$ and $g\Omega/\Gamma > 10$, the relation between polarization angle and magnetic field direction hold to within $\sim$15°. This improves quickly to better than $\sim$5° when $g\Omega/\Gamma$ becomes larger. We are thus in the regime where the polarization vectors directly determine the magnetic field direction, but adopt an additional 5° uncertainty in our determinations of the magnetic field direction on the plane of the sky.

For H_2O masers, it has been shown to be possible to estimate the saturation level, as determined by the emerging brightness temperature $T_{\rm b}\Delta\Omega$, and the intrinsic maser linewidth $\Delta V_{\rm i}$ by fitting both the total intensity and linear polarization maser spectra (Vlemmings et al. 2006a). As $T_{\rm b}\Delta\Omega$ determines the relation between $P_{\rm l}$ and θ, we are then able to constrain θ using the measured $P_{\rm l}$ and thus provide the full three-dimensional magnetic field direction. We have adapted the same modelling tools used for the 22-GHz H_2O masers to model the 6.7-GHz methanol maser transition.

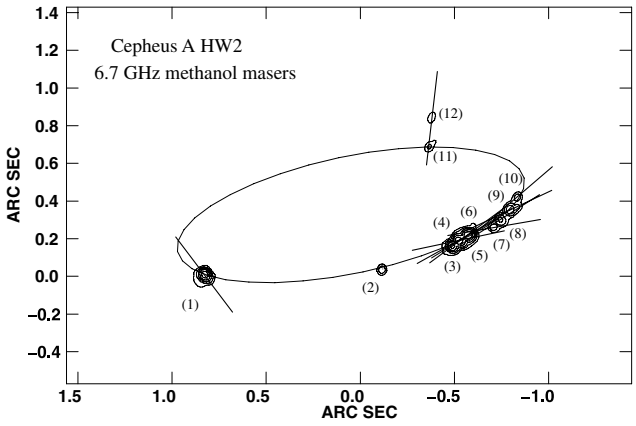

Figure 1. Total intensity (I) map of the 6.7-GHz methanol masers around Cepheus A HW2. Contours are drawn at 5, 10, 20, 40 and 80 Jy beam^{-1}. The labels identify the features presented in Tables 1 and 2. The vectors indicate the observed polarization angle χ. Also indicated is the best-fitting ellipse to the methanol maser feature distribution observed with MERLIN.

4 RESULTS

4.1 Maser distribution

The resulting velocity integrated image of the 6.7-GHz methanol masers around Cepheus A HW2 is shown in Fig. 1. No maser emission was detected at $<$5 Jy beam^{-1}. The 12 maser features that were identified are shown in Fig. 2 and presented in Table 1 with position offsets ($\Delta\alpha$ and $\Delta\delta$), velocity ($V_{\rm LSR}$), peak flux ($I_{\rm peak}$), fractional linear polarization ($P_{\rm l}$) and polarization angle (χ).

The 6.7-GHz methanol masers make up a nearly perfect elliptical distribution around HW2 and its disc, and the maser distribution observed with MERLIN matches that seen in European VLBI Network (EVN) and Japanese VLBI Network (JVN) observations (Sugiyama et al. 2008a; Torstensson et al., in preparation). A least-square fit of an ellipse to the MERLIN data indicates that the masers occur in a ring with a radius of $\sim$650 au, a thickness of $\sim$300 au, a projection angle on the sky of $\phi = -78°$ and an inclination angle of $i = 71°$. The maser ring appears tilted with respect to the molecular ($R = 580$ au, $\phi = -56°$ and $i = 68°$) and dust disc ($R = 330$ au, $\phi = -59°$ and $i = 56°$). Observations at high resolution (9×7 mas^2) with the EVN further indicate that the maser velocities are best fit by infall towards HW2 at $\sim$1.7 km s^{-1} (Torstensson et al. 2008; Torstensson et al., in preparation). While the molecular disc rotates with a velocity of $\sim$5 km s^{-1} (Jiménez-Serra et al. 2007), no significant rotation is observed in the maser region.

4.2 Maser polarization and turbulent linewidth

We used the radiative transfer method described in Section 3 to determine the emerging brightness temperature, $T_{\rm b}\Delta\Omega$, and intrinsic linewidth, $\Delta V_{\rm i}$, of the observed maser features. As a direct fit requires a regular maser spectrum that does not suffer from blending, we were able to fit to seven of the masers around Cepheus A HW2. The results of the fits are shown in Figs 3 and 4 and are given in

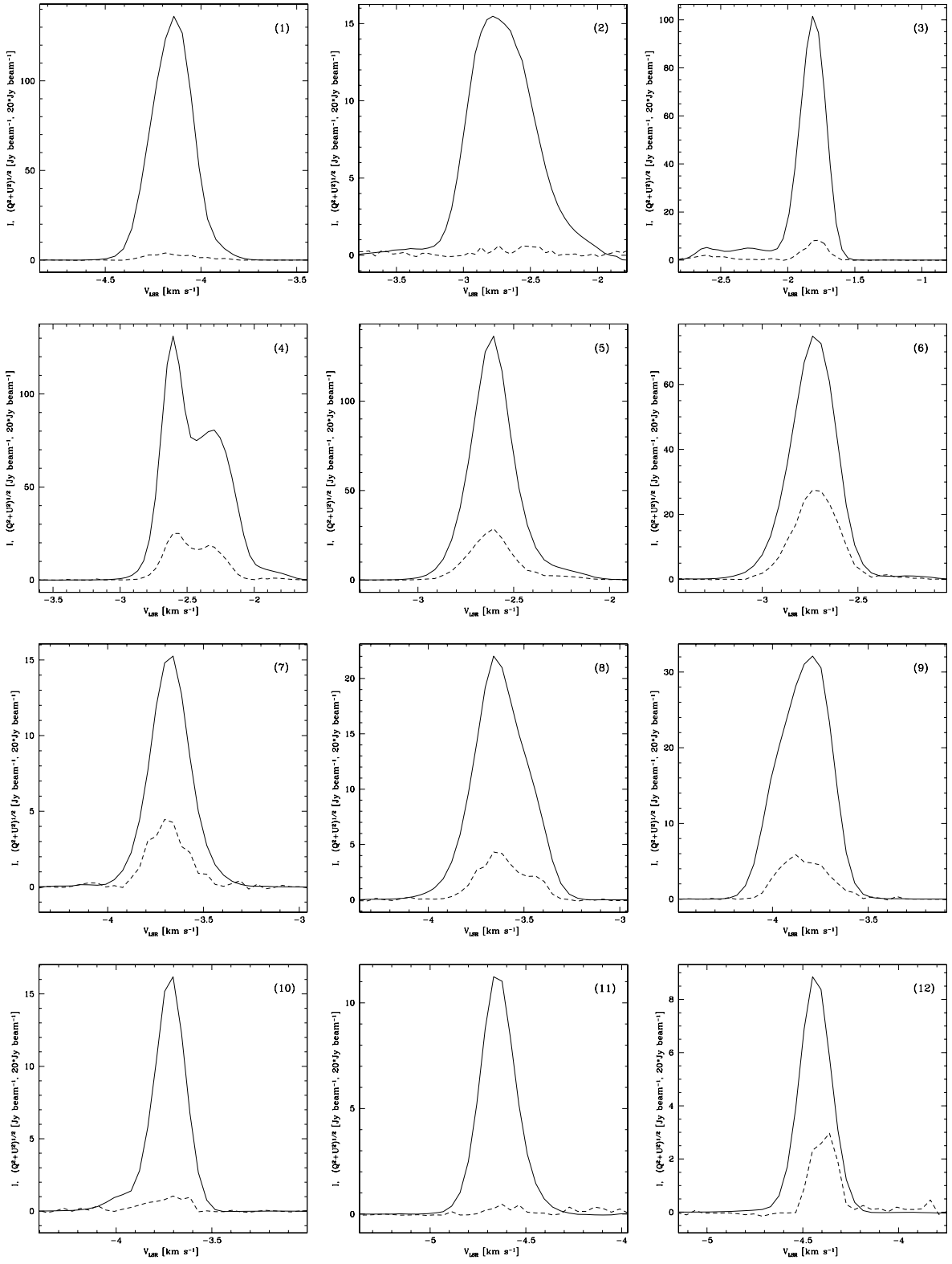

Figure 2. Total intensity (I; solid) and linear polarization (dashed) spectra for the 12 maser features detected above a level of 5 Jy beam^{-1} in the MERLIN observations. The linear polarization spectra have been multiplied by a factor of 20.

Table 2. They indicate an emerging brightness temperature in the range $10^8 < T_b \Delta\Omega < 10^9$ K sr, implying that the masers are not saturated, as the ratio of stimulated emission rate over decay rate $0.04 < R/\Gamma < 0.4$, and that our assumption for $\Delta\Omega$ in Section 3 is valid. It is worthwhile to note that our model calculations of the $T_b \Delta\Omega$ assume a maser decay rate of $\Gamma \sim 1\,s^{-1}$. However, the model emerging brightness temperature scale linearly with Γ and consequently the saturation level (R/Γ) does not change. The intrinsic

Table 1. Observation results.

Feature	$\Delta\alpha$ (arcsec)[a]	$\Delta\delta$ (arcsec)[a]	$V_{\rm LSR}$ (km s^{-1})	$I_{\rm peak}$ (Jy beam^{-1})	$P_{\rm l}$ (per cent)	χ ($^\circ$)
1	0.826	0.010	−4.14	136.1	0.15 ± 0.02	37 ± 6
2	−0.113	0.038	−2.78	15.5	<0.75	–
3	−0.489	0.161	−1.82	101.5	0.40 ± 0.06	-79 ± 2
4	−0.528	0.189	−2.30	131.1	1.10 ± 0.08	-65 ± 10
5	−0.564	0.212	−2.60	136.3	1.01 ± 0.03	-56 ± 2
6	−0.593	0.228	−2.73	74.8	1.88 ± 0.05	-56 ± 4
7	−0.710	0.270	−3.68	15.3	1.48 ± 0.07	-80 ± 2
8	−0.739	0.308	−3.65	22.0	1.02 ± 0.07	-61 ± 3
9	−0.805	0.356	−3.79	32.1	1.04 ± 0.15	-65 ± 1
10	−0.830	0.430	−3.70	16.2	0.41 ± 0.02	-49 ± 2
11	−0.364	0.687	−4.66	11.2	<0.84	–
12	−0.379	0.845	−4.55	8.8	1.65 ± 0.34	-3 ± 4

[a]Position offsets with respect to $\alpha = 22^{\rm h}56^{\rm m}17^{\rm s}.98$, $\delta = 62^\circ01'49''.390$.

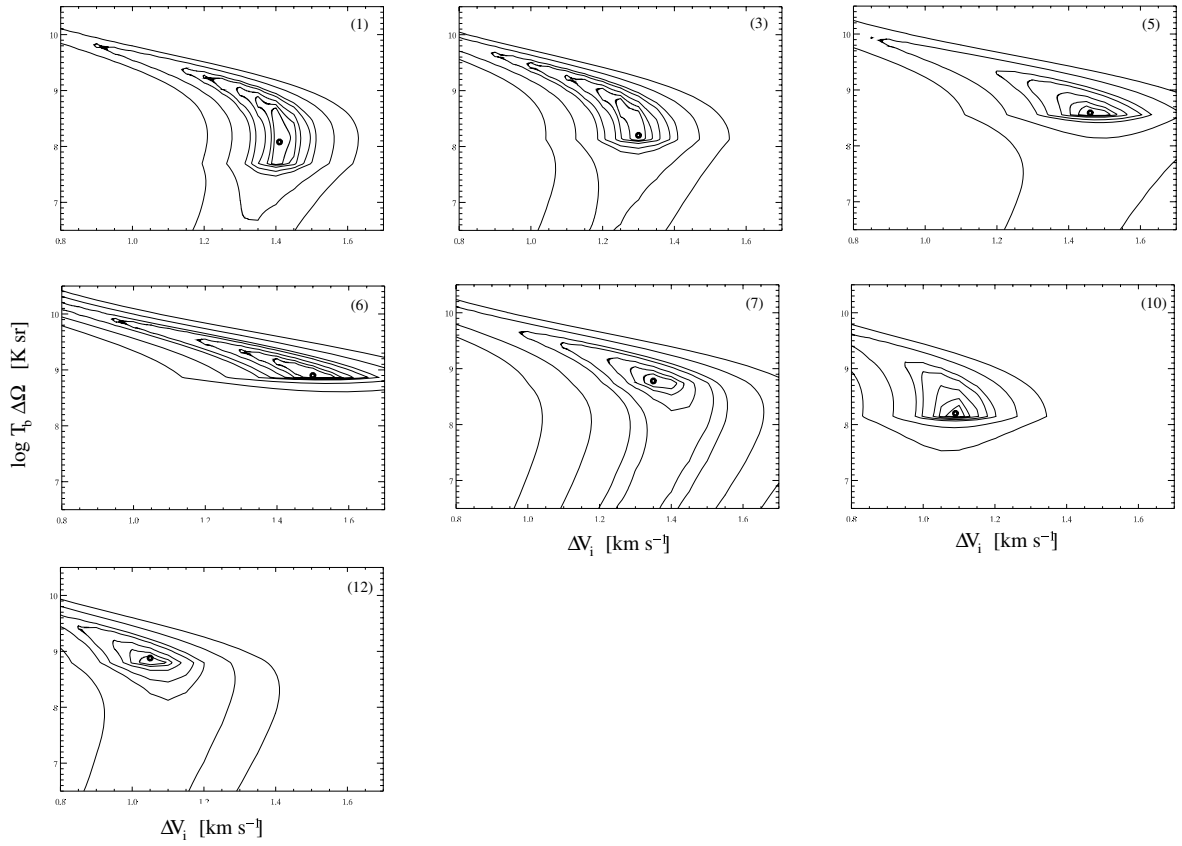

Figure 3. Results of the full radiative transfer χ^2-model fits, for those maser features from Fig. 2 that do not suffer from blending and for which linear polarization was detected. The fits yield the emerging maser brightness temperature $T_{\rm b}\Delta\Omega$ and intrinsic maser linewidth $\Delta V_{\rm i}$. Contours indicate the significance intervals $\Delta\chi^2 = 0.25, 0.5, 1, 2, 3, 7$, with the thick solid contour indicating the 1σ area.

maser linewidth lies in the range $1.0 < \Delta V_{\rm i} < 1.5\,{\rm km\,s^{-1}}$, with a weighted average $\Delta V_{\rm i} = 1.3 \pm 0.2\,{\rm km\,s^{-1}}$, which is much larger than the observed linewidth of $<0.3\,{\rm km\,s^{-1}}$ and shows that rebroadening, as a result of maser saturation, has not occurred yet. As the temperature needed to excite the 6.7-GHz masers is ∼200 K (Cragg, Sobolev & Godfrey 2005), the thermal linewidth is $\sim 0.7\,{\rm km\,s^{-1}}$. The intrinsic linewidth is thus significantly broader due to turbulence in the maser region and we estimate the turbulent linewidth to be $\Delta V \approx 1.1\,{\rm km\,s^{-1}}$.

Using the observed $P_{\rm l}$ and the fitted emerging brightness temperature, we were then able to determine the angle between the magnetic field and the maser propagation direction θ. The quoted errors on θ are the most compact 68 per cent probability interval, determined by analysing the full probability distribution function. For those maser features where no radiative transfer fit was possible, including the features without detected linear polarization, we have used the range of brightness temperatures as suggested by the fitted maser features. The inclination angles θ as well as the angle on the plane of the sky ϕ_B for the maser features are given in Table 2. The errors in ϕ_B are determined from the polarization angle χ, with an added uncertainty of 5° as described in Section 3. As seen in Table 2 and shown in Fig. 4, θ is constrained to $\theta > \theta_{\rm crit}$ at better than 1σ

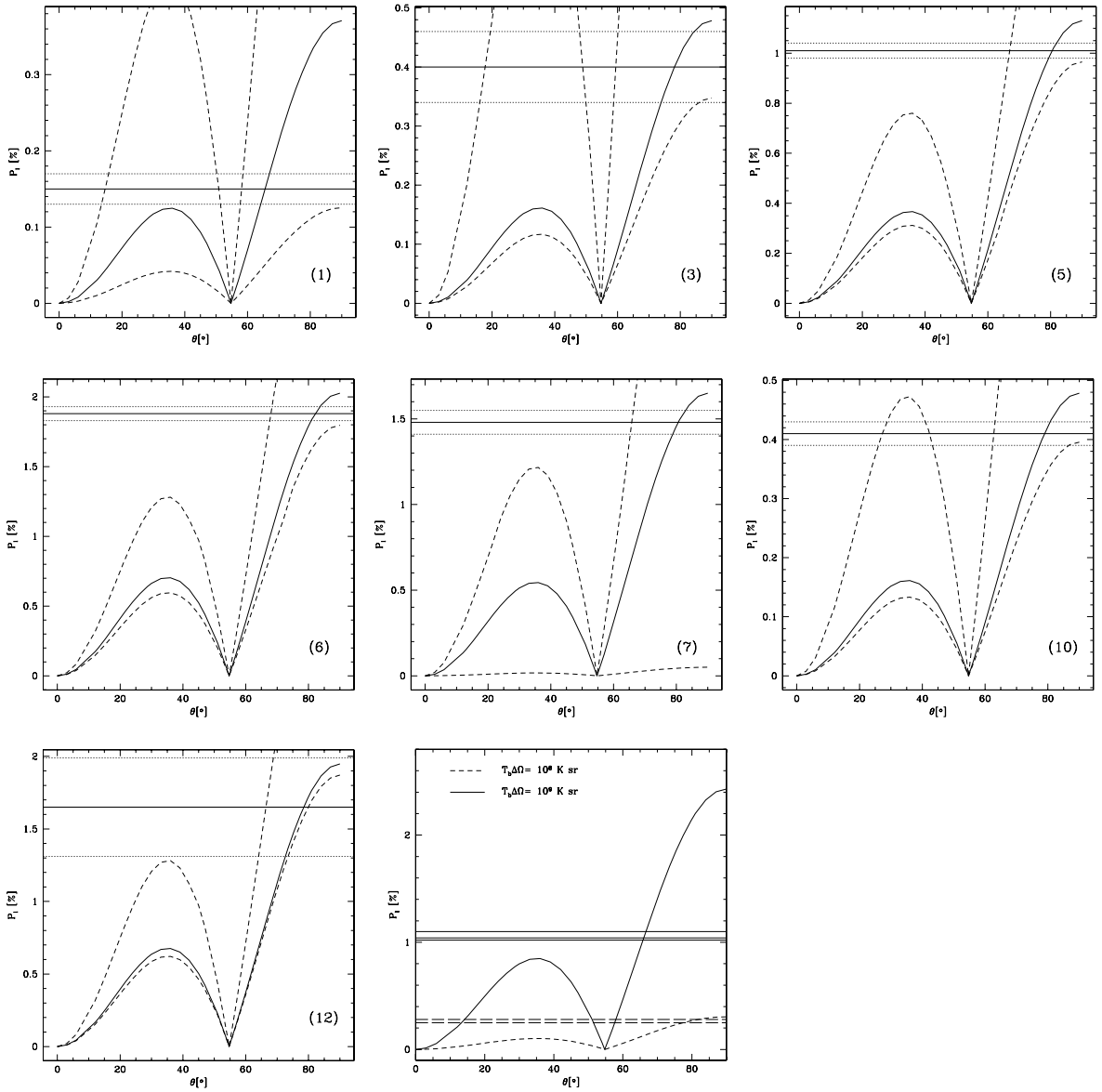

Figure 4. The angle θ between the maser propagation direction and the magnetic field versus the fractional linear polarization P_l. Panels are presented for the seven maser features for which an accurate fit could be made to the line profiles. The solid curves indicate the best-fitting emerging brightness temperatures and the dashed curves are the $\pm 1\sigma$ intervals. The horizontal solid and dashed lines are the measured polarization fraction and the corresponding errors. The last panel indicates the remaining five maser features with curves for typical emerging brightness temperatures. In this panel, the dashed horizontal lines are the 3σ upper limits for the maser features without measured polarization, as these limits provide strong constraints on θ.

level for the all but three of the maser features. Of those three, the best-fitting θ for features 3 and 10 are still larger than $\theta_{\rm crit}$. For the majority of the maser features, the magnetic field is thus likely perpendicular to the measured polarization vectors. Only for feature 1, the best-fitting θ is less than $\theta_{\rm crit}$, meaning that the magnetic field is more likely parallel to χ.

5 DISCUSSION

5.1 Methanol masers and the discs of Cepheus A HW2

As noted in Section 4.1, the 6.7-GHz methanol masers lie in an elliptical distribution around the molecular and dust discs of Cepheus A HW2. The masers are found at 650 au, outside the molecular disc with a radius of 580 au. The maser distribution also appears $\sim 20^\circ$ tilted with respect to the dust and molecular discs and shows no sign of rotation. This indicates that the masers are not part of the molecular disc itself. The temperature needed to maintain the masing conditions, $T_{\rm k} \sim 200$ K (Cragg et al. 2005), is slightly less than the $T = 250 \pm 30$ K found in the outer regions of the molecular disc (Jiménez-Serra et al. 2009). Furthermore, the hydrogen number density in the maser region, $n_{\rm H_2} \sim 10^9$ cm^{-3} (Cragg et al. 2005), is approximately three orders of magnitude less than that in the disc (Jiménez-Serra et al. 2009). Finally, the masers exhibit signs of infall and their velocity range covers only ~ 3 km s^{-1}, which indicates that it is unlikely that they are part of the Cepheus A HW2 outflow. We thus suggest that the maser, while not associated with the disc directly, probe material that is being accreted on to the disc from the surrounding medium.

Table 2. Fit results.

Feature	ΔV_i (km s^{-1})	$T_b \Delta\Omega$ (log K sr)	θ (°)	ϕ_B (°)
1	$1.41^{+0.04}_{-0.08}$	$8.08^{+0.58}_{-0.47}$	47^{+27}_{-24}	37 ± 11
3	$1.30^{+0.06}_{-0.11}$	$8.20^{+0.78}_{-0.16}$	68^{+7}_{-45}	11 ± 7
4	–	–	73^{+11}_{-9}	25 ± 15
5	$1.46^{+0.07}_{-0.17}$	$8.59^{+0.35}_{-0.08}$	73^{+16}_{-10}	34 ± 7
6	$1.50^{+0.18}_{-0.08}$	$8.90^{+0.35}_{-0.08}$	77^{+10}_{-7}	34 ± 9
7	$1.35^{+0.11}_{-0.11}$	$8.78^{+0.43}_{-1.59}$	74^{+15}_{-9}	10 ± 7
8	–	–	72^{+13}_{-9}	29 ± 8
9	–	–	72^{+14}_{-9}	25 ± 6
10	$1.09^{+0.04}_{-0.10}$	$8.20^{+0.50}_{-0.08}$	65^{+23}_{-25}	41 ± 7
12	$1.05^{+0.05}_{-0.14}$	$8.90^{+0.27}_{-0.08}$	72^{+8}_{-10}	87 ± 9

5.2 The magnetic field strength

Dynamic range limits in our MERLIN observations did not enable us to directly determine the magnetic field strength on the individual maser features around Cepheus A HW2, and we obtained a 3σ limit of $\sim$20 mG for the line-of-sight magnetic field. However, the magnetic field strength in the methanol maser region of Cepheus A was measured using the Effelsberg 100-m telescope (Vlemmings 2008). Through Zeeman splitting observations, the line-of-sight field strength was determined to be $B_{||} = B\cos(\theta) = 8.1 \pm 0.2$ mG (Vlemmings 2008), which is mostly constant across the full maser spectrum. As this value is a flux averaged magnetic field determined with a single dish telescope, we need to determine the amount of flux recovered and the number of maser features detected in our higher resolution MERLIN observations, to evaluate if the field measurement can be taken to be representative of the observed maser features. In Fig. 5, we show the comparison between the MERLIN and Effelsberg spectra. It is clear that the shape of the maser spectrum has changed significantly between the two epochs, though all individual maser features found with MERLIN can be identified in the Effelsberg spectrum. The change of the relative flux of the individual maser features was noted in Sugiyama et al. (2008b), who monitored Cepheus A with the Yamaguchi 32-m telescope. Comparing our spectra with their fig. 1 shows that the MERLIN spectrum is remarkably similar to what was observed on 2007 August 12, with no more than 10 per cent of the flux resolved out at high angular resolution. The MERLIN observations recover almost all of the single dish maser flux, and all features in the Effelsberg observations can be identified at high angular resolution. We can thus conclude that the Effelsberg magnetic field measurement can be taken as representative for true line-of-sight magnetic field in the maser region.

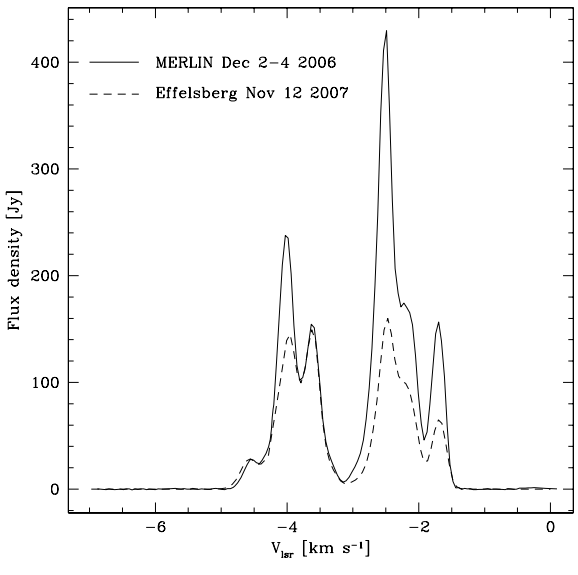

Figure 5. Total intensity spectra of the MERLIN observations (solid line) and the Effelsberg observations (dashed line) that were used to determine the magnetic field strength in the 6.7-GHz methanol maser region (Vlemmings 2008).

As discussed in Vlemmings (2008), there remains an estimated 25 per cent uncertainty on the magnetic field strength due to the unknown accuracy of the Zeeman splitting coefficient of the 6.7-GHz methanol maser transition. In addition to the measurement error of 0.2 mG on the magnetic field determination, we thus add an additional 2 mG uncertainty to the magnetic field strength when we determine the effect of the magnetic field around Cepheus A HW2.

5.3 Magnetic field morphology

The full three-dimensional magnetic field orientation was inferred using maser radiative transfer models described in Section 3 and is shown in Fig. 6. With the exception of one of the maser features that originates from the mid-plane of the molecular disc behind the outflow, the inferred magnetic field in the plane of the sky is perpendicular to the molecular and dust discs with an rms weighted average angle $\phi_B = 26° \pm 12°$. Moreover, the error weighted average angle between the magnetic field and the line of sight $\theta = 73° \pm 5°$ is consistent with the inclination of the molecular disc and the outflow. The overall magnetic field orientation angle corresponds closely to the magnetic field direction observed in the encompassing dust envelope (Curran & Chrysostomou 2007). The discrepant polarization angle found on the mid-plane maser feature is either due to the twisting of magnetic field lines towards the disc, or due to Faraday rotation caused by the ionized outflow. While the methanol masers at 6.7 GHz are not significantly affected by interstellar Faraday rotation, an electron density of $\sim$200 cm^{-3} along a short 100-au path through the ionized outflow with a few mG magnetic field can cause the observed polarization angle of the masers behind the outflow to rotate by more than 10°.

5.4 The role of the magnetic field

Since we have obtained the angle between the magnetic field and the line of sight, we can directly determine the magnetic field strength around the protostellar disc. For $B_{||} = 8.1 \pm 0.2 \pm 2$ mG and $\theta = 73° \pm 5°$, the absolute field strength $|B| = 23^{+9}_{-7}$ mG. From this, we can calculate a number of parameters to assess the role of the magnetic field during the massive protostellar collapse. The Alfvénic Mach number $m_a = \sigma\sqrt{3}/V_A$, where $\sigma = \Delta V/\sqrt{8\ln 2}$ and ΔV is the turbulent linewidth. The fits to the radiative transfer models indicate that the intrinsic maser linewidth is much larger than the thermal linewidth expected in the maser region with a typical kinetic temperature $T_k \sim 200$ K. Assuming the intrinsic linewidth to be broadened due by turbulent motions, we find that $\Delta V \sim 1.1$ km s^{-1}. In the methanol maser region with a hydrogen number density $n_{H_2} \sim 10^9$ cm^{-3}, the Alfvén velocity $V_A = |B|/\sqrt{4\pi\rho} = 2.05$ km s^{-1}. The measured infall motions, at 1.7 km s^{-1}, are thus

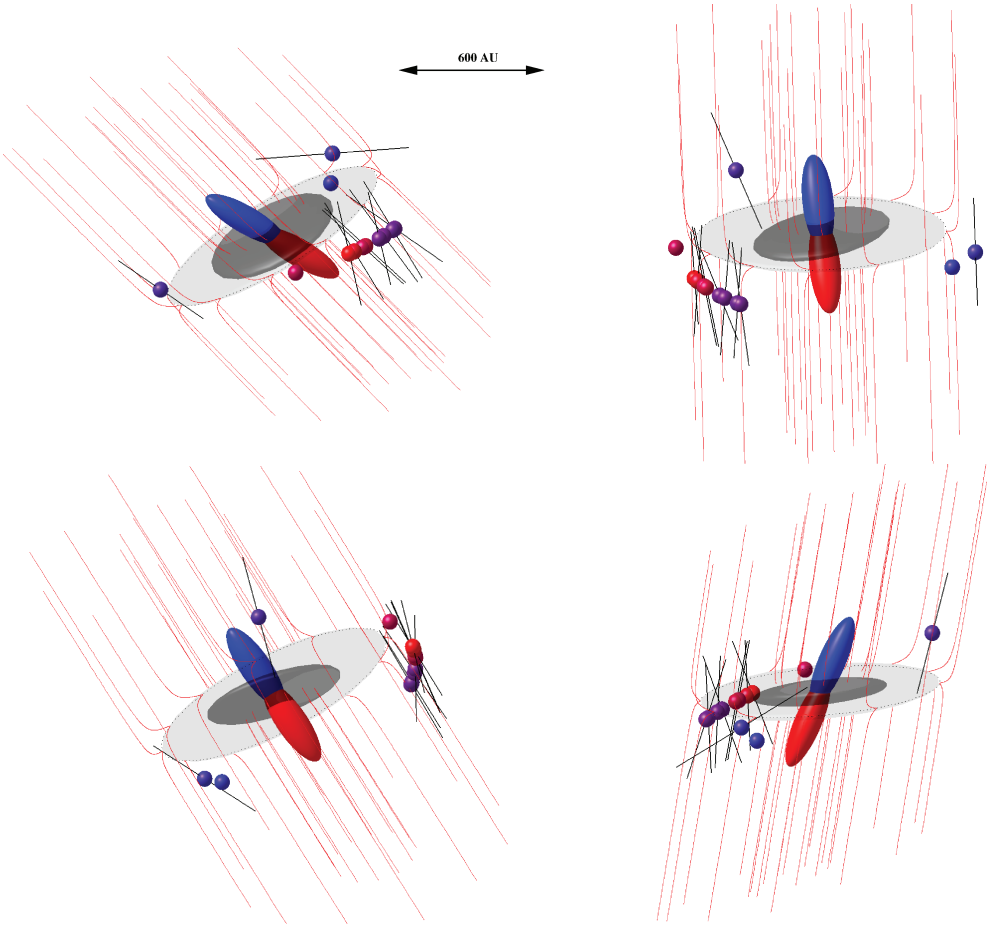

Figure 6. The three-dimensional magnetic field structure around the massive protostar Cepheus A HW2. The top left-hand panel corresponds to a viewing angle close to the observations while the three further panels have different viewing angles. Spheres indicate the masers, with the black vectors indicating the true magnetic field direction. The maser features are colour coded according to their velocity. The molecular disc (Patel et al. 2005) is indicated by the dashed line and light-grey structure while the dust disc (Patel et al. 2005; Jiménez-Serra et al. 2007) corresponds to the dark-grey ellipse. The blue- and redshifted lobes of the collimated radio outflow (Curiel et al. 2006) are also shown. The red lines indicate the proposed magnetic field morphology.

slightly sub-Alfvénic and $m_a = 0.4$. At 200 K, the sonic Mach number $m_s = 1.1$, and consequently, the ratio between thermal and magnetic energy $\beta = 2(m_a/m_s)^2 = 0.27$. The magnetic field dominates the energies in the high-density protostellar environment probed by the masers.

We can also calculate the mass to magnetic flux ratio M/Φ compared to the critical value of this ratio $\lambda = (M/\Phi)/(M/\Phi)_{crit}$. The critical value $(M/\Phi)_{crit} = c_\Phi/\sqrt{G} \approx 0.12/\sqrt{G}$ (Mouschovias & Spitzer 1976; Tomisaka, Ikeuchi & Nakamura 1988) is taken from numerical models for the collapse of a spherical molecular cloud into a highly flattened structure and defines the critical mass that can be supported against collapse by the magnetic field. When $\lambda < 1$, the magnetic field prevents collapse, but when λ becomes larger than 1, gravity overwhelms the magnetic field. In terms of hydrogen column density, λ can be determined from $\lambda = 7.6 \times 10^{-24}\, N(H_2)/|B|$, with the magnetic field in mG. Taking the maser region to be ~300-au thick, as determined by our observations, the hydrogen column density along the magnetic field lines is $N(H_2) \approx 5 \times 10^{24}$ cm^{-2}. This yields $\lambda = 1.7^{+0.7}_{-0.5}$, indicating that the region is slightly supercritical, a condition needed for the collapse to proceed. Similar values for λ were found using large-scale Zeeman splitting observations of an ensemble of molecular clouds (Crutcher 1999). However, as those observations lacked the three-dimensional magnetic field information, the results were uncertain by order a factor of 2, making it impossible to distinguish between sub- and supercritical cloud cores.

Finally, comparing the methanol maser magnetic field strength with other field strength measurements in the high-density region around HW2 ($n_{H_2} > 10^5$ cm^{-3}), we find that the field scales approximately as $B \propto n_{H_2}^{0.5}$ (fig. 3 from Vlemmings 2008). This relation could be the consequence of ambipolar diffusion, but it also naturally occurs for the collapse of a spherical cloud with frozen in field lines, when the preferred infall direction is along the magnetic field. Such a collapse forms a flattened disc-like structure similar to as observed around HW2. We thus suggest that the magnetic field plays a crucial role in regulating the final stages of the formation of the massive protostar Cepheus A HW2, as is commonly expected during low-mass star formation.

5.5 Future perspectives

5.5.1 Cepheus A as a prototype methanol maser source?

Because of their distance and complexity, the relation between the methanol masers and the protostellar environment for most other maser sources is still unknown. However, Zeeman splitting

observations have shown typical magnetic field strengths along the line of sight of ∼12 mG in over 70 per cent of the observed methanol maser sources (Vlemmings 2008). Strong and dynamically important magnetic fields are thus present in most massive star-forming region traced by methanol masers. Furthermore, a recent survey has revealed that ∼30 per cent of the methanol maser sources display an elliptical structure (Bartkiewicz et al. 2009). This suggests that the methanol masers of a large fraction of star-forming regions are located in an interface between a disc or torus and the infalling material, similar to the inferred origin of the masers around Cepheus A. Our picture of magnetic field regulated infall and accretion towards Cepheus A HW2 thus potentially describes a large number of massive star-forming regions.

5.5.2 Further e-MERLIN observations

With the e-MERLIN upgrade (Garrington et al. 2004), it will soon be possible to map multiple maser transitions simultaneously with the radio continuum. By observing in full polarization mode, this will allow for a direct comparison between the magnetic field structure determined from the masers and the continuum morphology. Single track observations will allow for mapping of massive star-forming regions at different evolutionary stages down to a continuum sensitivity approaching 3 μJy beam^{-1}. Simultaneously, the sensitivity in a narrow 6.7-GHz maser frequency band will then be sufficient to detect linear polarization for >75 per cent of the star-forming regions with methanol masers, when assuming the flux analysis of van der Walt (2005). When analysed in a similar way to the Cepheus A HW2 observations presented here, such observations have the potential to significantly further our understanding of the magnetic field around massive protostars.

6 CONCLUSION

We have demonstrated the power of maser polarization observation, and particularly those using methanol masers, in deducing the full three-dimensional strength and structure of the magnetic field around massive protostars. The detection of a coherent magnetic field direction in maser features that individually have a size of a few au, suggests that the masers do not probe isolated pockets of a shock-compressed magnetic field. In that case, the polarization direction would be determined by the direction of compression for each maser individually and observing coherent polarization angles would be unlikely. A similar conclusion could be drawn from recent observations of W75N at high angular resolution with the EVN that reveal a uniform magnetic field direction in individual methanol maser features spread over ∼2000 au (Surcis et al. 2009). The detection of a large-scale magnetic field is further confirmed by the good agreement of the field direction with that determined using dust polarization observations of the entire Cepheus A region. The three-dimensional magnetic field geometry around Cepheus A HW2 supports the theories in which magnetic fields regulate the infall and outflow close to massive protostars in a similar way as during low-mass star formation, even if the high-mass star-forming regions are considerably more complex. The strong magnetic field that appears to be threading the disc will play a crucial role in maintaining the high accretion rate needed during massive star formation and is potentially essential in maintaining disc stability and creating the conditions to allow for planet formation (Johansen & Klahr 2005; Wardle 2007; Johansen & Levin 2008).

ACKNOWLEDGMENTS

WHTV acknowledges support by the Deutsche Forschungsgemeinschaft (DFG) through the Emmy Noether Research grant VL 61/3-1. GS is a member of the International Max Planck Research School (IMPRS) for Astronomy and Astrophysics at the Universities of Bonn and Cologne. KJET was supported by the EU Framework 6 Marie Curie Early Stage Training programme under contract number MEST-CT-2005-19669 'ESTRELA'.

REFERENCES

Banerjee R., Pudritz R. E., 2007, ApJ, 660, 479
Bartkiewicz A., Szymczak M., Cohen R. J., Richards A. M. S., 2005, MNRAS, 361, 623
Bartkiewicz A., Szymczak M., van Langevelde H. J., Richards A. M. S., Pihlström Y. M., 2009, A&A, 502, 155
Basu S., Mouschovias T. C., 1994, ApJ, 432, 720
Bonnell I. A., Bate M. R., 2005, MNRAS, 362, 915
Bonnell I. A., Bate M. R., Zinnecker H., 1998, MNRAS, 298, 93
Comito C., Schilke P., Endesfelder U., Jiménez-Serra I., Martín-Pintado J., 2007, A&A, 469, 207
Cragg D. M., Sobolev A. M., Godfrey P. D., 2005, MNRAS, 360, 533
Crutcher R. M., 1999, ApJ, 520, 706
Curiel S. et al., 2006, ApJ, 638, 878
Curran R. L., Chrysostomou A., 2007, MNRAS, 382, 699
Deguchi S., Watson W. D., 1990, ApJ, 354, 649
Figer D. F., Najarro F., Morris M., McLean I. S., Geballe T. R., Ghez A. M., Langer N., 1998, ApJ, 506, 384
Garrington S. T. et al., 2004, Proc. SPIE, 5489, 332
Girart J. M., Beltrán M. T., Zhang Q., Rao R., Estalella R., 2009, Sci, 324, 1408
Goldreich P., Kwan J., 1974, ApJ, 190, 27
Goldreich P., Keeley D. A., Kwan J. Y., 1973, ApJ, 179, 111
Hughes V. A., Wouterloot J. G. A., 1984, ApJ, 276, 204
Jiménez-Serra I., Martín-Pintado J., Rodríguez-Franco A., Chandler C., Comito C., Schilke P., 2007, ApJ, 661, L187
Jiménez-Serra I., Martín-Pintado J., Caselli P., Martín S., Rodríguez-Franco A., Chandler C., Winters J. M., 2009, ApJ, 703, L157
Johansen A., Klahr H., 2005, ApJ, 634, 1353
Johansen A., Levin Y., 2008, A&A, 490, 501
McKee C. F., Tan J. C., 2003, ApJ, 585, 850
Menten K. M., Reid M. J., Pratap P., Moran J. M., Wilson T. L., 1992, ApJ, 401, L39
Minier V., Booth R. S., Conway J. E., 2002, A&A, 383, 614
Moscadelli L., Reid M. J., Menten K. M., Brunthaler A., Zheng X. W., Xu Y., 2009, ApJ, 693, 406
Mouschovias T. C., Spitzer L., Jr, 1976, ApJ, 210, 326
Nedoluha G. E., Watson W. D., 1990, ApJ, 354, 660
Nedoluha G. E., Watson W. D., 1991, ApJ, 367, L63
Patel N. A. et al., 2005, Nat, 437, 109
Scappaticci G. A., Watson W. D., 1992, ApJ, 387, L73
Shu F. H., Najita J., Ostriker E. C., Shang H., 1995, ApJ, 455, L155
Sugiyama K., Fujisawa K., Doi A., Honma M., Kobayashi H., Bushimata T., Mochizuki N., Murata Y., 2008a, PASJ, 60, 23
Sugiyama K., Fujisawa K., Doi A., Honma M., Isono Y., Kobayashi H., Mochizuki N., Murata Y., 2008b, PASJ, 60, 1001
Surcis G., Vlemmings W. H. T., van Langevelde H. J., Dodson R., 2009, A&A, 506, 757
Tomisaka K., Ikeuchi S., Nakamura T., 1988, ApJ, 335, 239
Torrelles J. M., Patel N. A., Curiel S., Ho P. T. P., Garay G., Rodríguez L. F., 2007, ApJ, 666, L37
Torstensson K., van Langevelde H. J., Vlemmings W., van der Tak F., 2008, in Proc. 9th European VLBI Network Symposium, p. 39
van der Walt J., 2005, MNRAS, 360, 153

Vlemmings W. H. T., 2007, in Chapman J. M., Baan W. A., eds, Proc. IAU Symp. 242, Astrophysical Masers and their Environment. Cambridge Univ. Press, Cambridge, p. 37
Vlemmings W. H. T., 2008, A&A, 484, 773
Vlemmings W. H. T., van Langevelde H. J., 2005, A&A, 434, 1021
Vlemmings W. H. T., Diamond P. J., van Langevelde H. J., Torrelles J. M., 2006a, A&A, 448, 597
Vlemmings W. H. T., Harvey-Smith L., Cohen R. J., 2006b, MNRAS, 371, L26
Wardle M., 2007, Ap&SS, 311, 35
Watson W. D., 2002, in Migenes V., Reid M. J., eds, Proc. IAU Symp. 206, Cosmic Masers: From Proto-Stars to Black Holes. Astron. Soc. Pac., San Francisco, p. 464
Wolfire M. G., Cassinelli J. P., 1987, ApJ, 319, 850
Zinnecker H., Yorke H. W., 2007, ARA&A, 45, 481

This paper has been typeset from a TEX/LATEX file prepared by the author.